

## Identification of inertial modes in the solar convection zone

SANTIAGO A. TRIANA <sup>1</sup>, GUSTAVO GUERRERO <sup>2,3</sup>, ANKIT BARIK <sup>4</sup> AND JÉRÉMY REKIER <sup>1,5</sup>

<sup>1</sup>*Royal Observatory of Belgium, Ringlaan 3, 1180 Brussels, Belgium*

<sup>2</sup>*Federal University of Minas Gerais, Av. Pres. Antônio Carlos, 6627, Belo Horizonte, MG, 31270-901, Brazil*

<sup>3</sup>*New Jersey Institute of Technology, Newark, NJ 07102 USA*

<sup>4</sup>*Johns Hopkins University, 3400 N. Charles Street, Baltimore, MD 21210, USA*

<sup>5</sup>*Department of Earth and Planetary Science, University of California, Berkeley, CA 94720, USA*

Submitted to ApJL

### ABSTRACT

The observation of global acoustic waves (p modes) in the Sun has been key to unveil its internal structure and dynamics. A different kind of waves, known as sectoral Rossby modes, have been observed and identified relatively recently, which potentially opens the door to probe internal processes that are inaccessible through p mode helioseismology. Yet another set of waves, appearing as retrograde-propagating, equatorially antisymmetric vorticity waves, have been observed very recently but their identification remained elusive. Here, through a numerical model implemented as an eigenvalue problem, we provide evidence supporting the identification of those waves as inertial eigenmodes, of a class distinct from Rossby modes, with substantial amplitudes deep in the solar convective zone. We also suggest that the signature of tesseral Rossby modes might be present in the recent observational data.

*Keywords:* Solar oscillations (1515) — Helioseismic pulsations (708) — Hydrodynamics (1963)

### 1. INTRODUCTION

The Coriolis forces in any rotating fluid body, from planetary cores and atmospheres to stars, support the presence of inertial waves. Rossby waves, common in the Earth's atmosphere, are a particular subset of inertial waves. In the astrophysical literature Rossby waves are referred to as *r-modes*, while the more general class of inertial waves are known, a bit confusingly, as *generalized r-modes* (Lockitch & Friedman 1999). Rossby waves play a fundamental role in the emission of gravitational waves in neutron stars (Andersson 1998), they have a major influence on Earth's weather (Michel & Rivière 2011), and may be even present in the fluid cores of terrestrial planets affecting their global rotation (Triana et al. 2021).

Retrograde-propagating vorticity waves, *symmetric* with respect to the equator, have been observed and identified a few years ago as Rossby waves in the Sun by Löptien et al. (2018) and further confirmed by Hathaway & Upton (2021). This discovery is highly relevant since Rossby waves are sensitive to turbulent flows, as opposed to the acoustic (p) modes also present in the

solar convective zone. Thus, the observation and careful characterization of solar Rossby waves might be instrumental for the understanding of the internal solar dynamics so far elusive for traditional p mode helioseismology.

More recently, Hanson et al. (2022) provided observational evidence of a distinct set of high-frequency, retrograde-propagating (HFR) vorticity waves, penetrating at least to 3% of the solar radius, but this time with an *antisymmetric* vorticity with respect to the equator. However, the identification of these waves was left as an open question. They do not seem to fit the classical Rossby wave dispersion relation that, contrastingly, worked so well for the symmetric-vorticity waves described by Löptien et al. (2018).

In this work we provide numerical evidence supporting the identification of the HFR waves as a class of inertial waves, different from Rossby modes, that span the whole convective zone depth. Our numerical model is based on a simplified physical description of the convection zone, providing the eigenvalues and eigenvectors associated with the inertial modes that it may support. We find modes with markedly low damping, with the

same propagation direction, same equatorial symmetry, same spherical harmonic spectra, and similar frequencies as the observed HFR waves.

Non-axisymmetric (i.e. with azimuthal wave number  $m \neq 0$ ) inertial eigenmodes drift in longitude according to their phase speed, so in this work we refer to them as waves or modes interchangeably.

## 2. A MODEL FOR INERTIAL EIGENMODES

### 2.1. Main description

A starting model for solar inertial oscillations can be built by representing the solar convection zone as a spherical shell filled with an homogeneous, incompressible, and viscous fluid. The inner radius  $r_c$  of the shell corresponds to the outer radius of the radiative core, with a value  $r_c \sim 0.71R_\odot$ ,  $R_\odot$  being the solar radius. The flow velocity associated with the vorticity waves in the convection zone is much smaller than  $\Omega_\odot R_\odot$ , where  $\Omega_\odot/2\pi = 453.1$  nHz is the Sun's rotation rate at the equator, thus the flow velocity  $\mathbf{u}$  can be described to a good approximation as a small perturbation to the uniformly rotating background flow by the *linear* Navier-Stokes equation:

$$\partial_t \mathbf{u} + 2\hat{\mathbf{z}} \times \mathbf{u} = -\nabla p + E\nabla^2 \mathbf{u}. \quad (1)$$

The variables in the preceding equation are rendered dimensionless by taking  $R_\odot$  and  $1/\Omega_\odot$  as the units for length and time, respectively. We use  $\hat{\mathbf{z}}$  as the unit vector along the solar spin axis, and  $p$  is the reduced pressure. We introduce also the Ekman number  $E$  as the ratio between the viscous diffusion time scale and the rotation time scale:

$$E = \frac{\nu_{\text{eff}}}{\Omega_\odot R_\odot^2}, \quad (2)$$

where  $\nu_{\text{eff}}$  is an *effective* or turbulent eddy viscosity. We use stress-free boundary conditions for both the inner and the outer boundaries of the shell. The flow velocity  $\mathbf{u}$  follows a time dependence described by

$$\mathbf{u}(\mathbf{r}, t) = \mathbf{u}_0(\mathbf{r})e^{\lambda t} + \text{cc}, \quad (3)$$

where  $\lambda = (\sigma/\Omega_\odot) - i(\omega/\Omega_\odot)$  is a complex number whose real part  $\sigma/\Omega_\odot$  corresponds to the dimensionless decay rate and the imaginary part  $\omega/\Omega_\odot$  to the dimensionless eigenfrequency. We add the complex conjugate (cc) to keep  $\mathbf{u}$  real. Then we write the velocity amplitude  $\mathbf{u}_0$  in the poloidal-toroidal decomposition:

$$\mathbf{u}_0 = \nabla \times \nabla \times [\mathcal{P}(\mathbf{r}) \mathbf{r}] + \nabla \times [\mathcal{T}(\mathbf{r}) \mathbf{r}]. \quad (4)$$

We use spherical harmonic expansions for the angular dependence of the scalar functions  $\mathcal{P}$ ,  $\mathcal{T}$ . For instance,

we write the toroidal scalar function  $\mathcal{T}(\mathbf{r})$  as

$$\mathcal{T}(r, \theta, \phi) = \sum_{l=1}^{l_{\text{max}}} \sum_{m=-l}^l T_{lm}(r) Y_l^m(\theta, \phi), \quad (5)$$

where  $Y_l^m$  are the spherical harmonics,  $T_{lm}(r)$  is a radial function, and  $l_{\text{max}}$  determines the angular truncation level. A completely analogous expression goes for  $\mathcal{P}(\mathbf{r})$ . The spherical harmonic expansion leads to a fully decoupled problem in the azimuthal wave number  $m$ , allowing us to consider a single  $m$  at a time. If  $m \neq 0$ , inertial eigenmodes are either retrograde or prograde, which is determined by the sign of their *phase speed*  $\omega/m$ . Note that the retrograde inertial eigenmode spectrum does not coincide in general with the prograde one.

Our numerical scheme involve expansions of the radial functions  $P_{lm}(r)$  and  $T_{lm}(r)$  in terms of Chebyshev polynomials. This allows us to write the problem represented by Eq. (1) as a generalized eigenvalue problem. For more details see Appendix A.

### 2.2. Symmetry considerations

The waves reported by Hanson et al. (2022) are described in terms of the radial vorticity observed near or at the solar surface. The spherical harmonic coefficients of the radial vorticity at any radius  $r$  are related in a simple way to the toroidal functions  $T_{lm}(r)$ :

$$[\hat{\mathbf{r}} \cdot (\nabla \times \mathbf{u}_0)]_{l,m} = l(l+1) \frac{T_{lm}(r)}{r}. \quad (6)$$

The velocity field  $\mathbf{u}$  of an inertial mode can be either equatorially symmetric or antisymmetric. Thus, the vorticity  $\nabla \times \mathbf{u}$  has the *opposite* equatorial symmetry as  $\mathbf{u}$ . Explicitly, if a mode is equatorially antisymmetric in the vorticity, it fulfills

$$\begin{aligned} u_r(r, \pi - \theta, \phi) &= u_r(r, \theta, \phi), \\ u_\theta(r, \pi - \theta, \phi) &= -u_\theta(r, \theta, \phi), \\ u_\phi(r, \pi - \theta, \phi) &= u_\phi(r, \theta, \phi), \end{aligned} \quad (7)$$

i.e. it is equatorially symmetric in the velocity. An inertial mode equatorially symmetric in velocity, with azimuthal wave number  $m$ , has poloidal functions  $P_{lm}$  with indices such that  $l = m, m+2, m+4, \dots$ , and the toroidal functions  $T_{lm}$  have indices such that  $l = m+1, m+3, \dots$ . Conversely when the mode is antisymmetric.

Inertial modes are a general class of modes that include Rossby modes (also known as *planetary waves*) as a subset. The analytical dispersion relation for Rossby modes, namely

$$\frac{\omega}{\Omega_\odot} = -\frac{2m}{l(l+1)}, \quad (8)$$

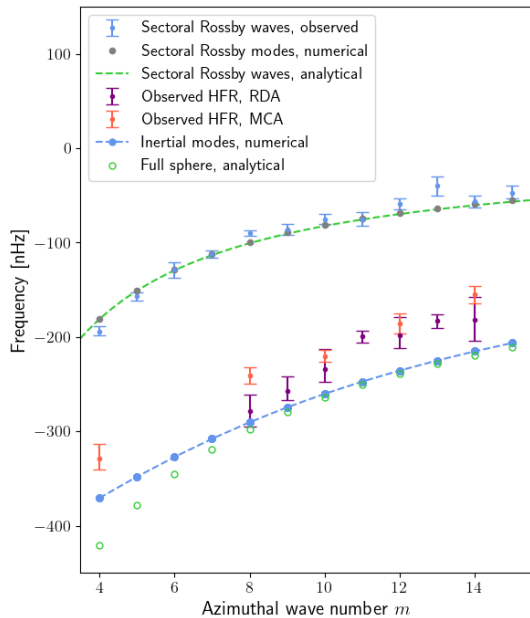


**Figure 1.** Observed HFR vorticity wave frequencies from mode-coupling analysis (MCA, orange error bars) and from ring-diagram analysis (RDA, purple error bars) compared to the inertial mode frequencies computed numerically for  $E = 1.06 \times 10^{-4}$  and  $r_c = 0.71R_\odot$  (blue dash line with dots). We include analytical, numerical, and observed sectoral Rossby mode frequencies for reference.

is usually derived assuming a thin spherical shell, which ignores motion in the radial direction, leaving only the toroidal part (see e.g. Rieutord 2014). In the ideal case, a Rossby mode has only one spherical harmonic  $Y_l^m$  component. These modes can then be classified as *sectoral* if  $l = m$ , or *tesseral* if  $l > m$ . A sectoral Rossby mode is by necessity equatorially antisymmetric in the velocity (i.e. symmetric in vorticity). These are the modes that have been observed and identified in the Sun by Löptien et al. (2018). Tesseral Rossby modes can have either symmetry. Similarly, a Rossby mode with an equatorially symmetric velocity (i.e. antisymmetric in vorticity) is thus a tesseral Rossby mode. When the shell is not thin, poloidal motions can become significant, the dispersion relation (8) is not generally valid, and the foregoing classification does not follow unmodified.

### 3. RESULTS

The line width  $\Gamma$  of the modes corresponds roughly to two times their decay rate constant  $\sigma$ , in analogy with a lightly damped harmonic oscillator. We have tuned the Ekman number so that the mean  $[\sigma]$  of numerically computed modes (the HFR candidates), from  $m = 8$  to  $m = 14$ , matches one half the mean  $[\Gamma]$  of the observed

line widths that were computed via ring-diagram analysis of Helioseismic and Magnetic Imager (HMI) measurements, as reported by Hanson et al. (2022) (see their Table 1, column 5). Thus,  $[\sigma] \approx [\Gamma]/2 = 19.5$  nHz is obtained when  $E = 1.06 \times 10^{-4}$ . We choose the outer radius of the radiative core at  $r_c/R_\odot = 0.71$ . We then proceed to calculate eigenfrequencies and eigenmodes for different values of  $m$ . The inertial mode frequency spectrum is dense, so there is always an inertial mode arbitrarily close to any frequency we might choose as a target for the eigensolver. However, their damping factor  $\sigma$  allows us to discriminate between lightly damped modes, i.e. ones that are more easily excited, usually with simpler spatial structures, against heavily damped ones, typically with more complex spatial structures. The *least* damped modes in a broad interval around the observed frequencies are plotted in Fig. 1 (blue dots - blue dashed line labeled ‘inertial modes, numerical’). These modes are retrograde-propagating ( $\omega < 0$ ), have equatorially antisymmetric radial vorticity (i.e. equatorially symmetric flow velocity) and their dominant spherical harmonic component,  $T_{lm}$ , near or at the solar surface is such that  $l = m + 1$ , matching the corresponding characteristics of the observed HFR vorticity waves. We have extracted the observed HFR frequencies in Fig. 1 (orange and purple error bars) from Table 1 and Table S1 of Hanson et al. (2022). For comparison, Fig. 1 also presents the sectoral Rossby mode frequencies obtained with our model, which we used for validation, and the sectoral Rossby modes observed by Löptien et al. (2018).

With the exception of the purely toroidal inertial eigenmodes, the eigenfrequencies are sensitive to the width of the shell cavity. In Fig. 2 we show the eigenfrequencies obtained with our numerical model by considering different radii for the outer radius of the radiative core  $r_c$  and different azimuthal wave numbers  $m$ . Symbol color and size indicates  $\log_{10} |\sigma/\Omega_\odot|$ , with larger, deep red symbols indicating modes with little damping, which are easier to excite, and smaller, green-turquoise symbols indicating heavily damped modes. We see in the figure eigenmodes with small magnitude frequencies, typically with  $|\omega/\Omega_\odot| < 0.3$ , particularly at low  $m$ , with very little damping. For instance, when  $m = 4$ , the least damped mode has a frequency of about  $\omega/\Omega_\odot \sim -0.2$  at  $r_c/R_\odot = 0.71$  which increases in magnitude for larger  $r_c$ . This class of modes have frequencies that generally decrease in magnitude and become more damped as  $m$  increases. These are tesseral *Rossby* modes whose frequencies are given to a very good approximation by the dispersion relation (8) but *only* when  $r_c/R_\odot \gtrsim 0.94$ , i.e. when the shell cavity is thin. The top, left panel in Fig. 2

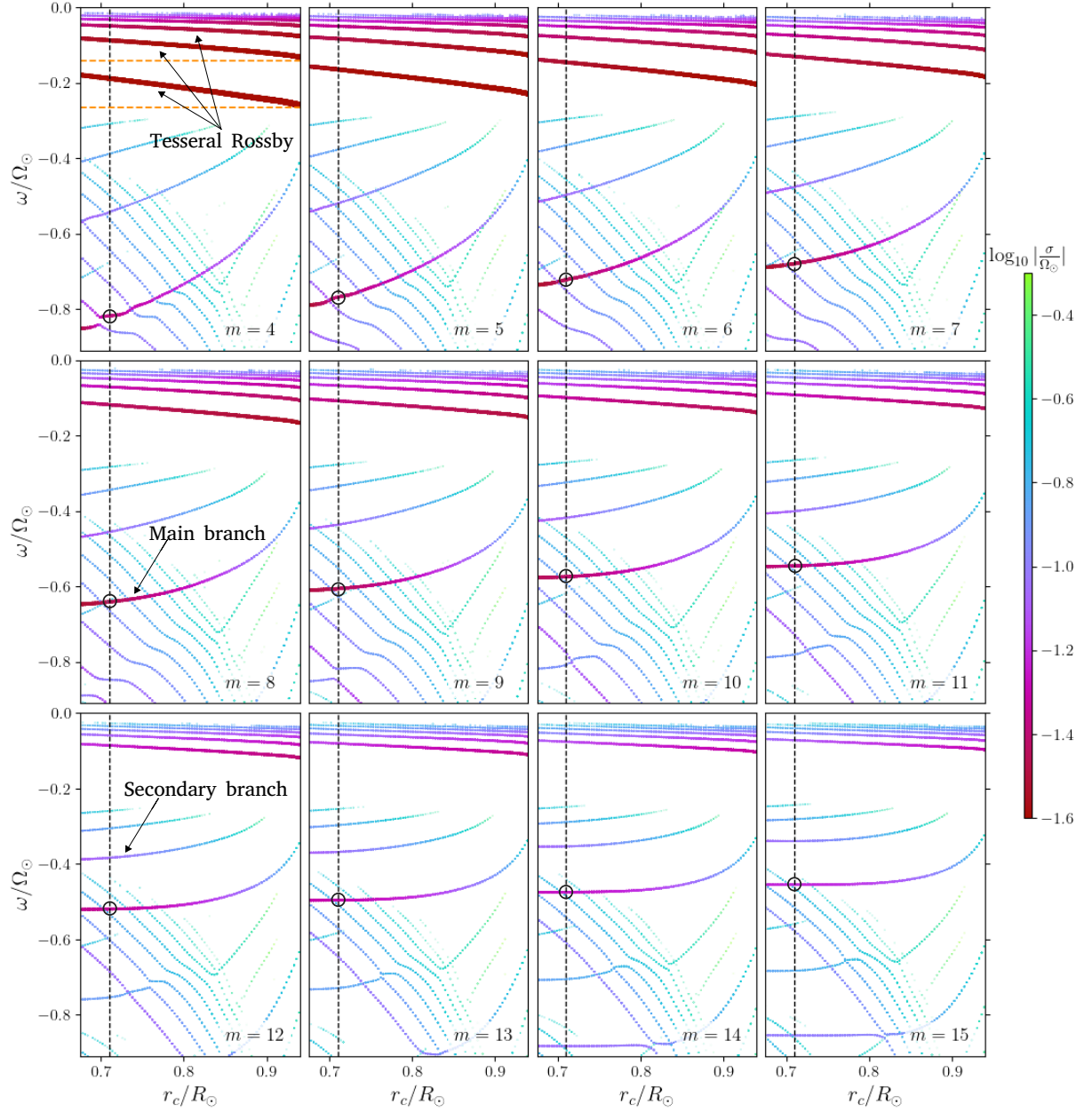


**Figure 2.** Eigenfrequencies of equatorially *antisymmetric vorticity* modes as a function of the radiative core outer radius  $r_c$  for different azimuthal wave numbers  $m$ . Color and symbol size indicates the eigenmodes' damping decay factor  $\sigma$  with larger deep-red points representing lightly damped modes (more likely to be excited), and smaller green-turquoise points representing heavily damped modes (less likely to be excited). The vertical black dashed line marks the Sun's radiative core outer radius at  $r_c = 0.71R_\odot$ . Black circles mark the modes we identify as the observed HFR waves. The horizontal orange dashed lines in the  $m = 4$  panel are the frequencies of the  $(l = 5, m = 4)$  and the  $(l = 7, m = 4)$  Rossby modes according to Eq. (8).

shows the theoretical frequencies of the ( $l = 5, m = 4$ ) and the ( $l = 7, m = 4$ ) Rossby modes from Eq. (8) as horizontal orange dash lines.

We want to draw attention now to the modes with frequencies near  $\omega/\Omega_\odot \sim -0.8$  for  $m = 4$ ,  $r_c/R_\odot = 0.71$ , progressively decreasing in magnitude as  $m$  increases until reaching  $\omega/\Omega_\odot \sim -0.45$  at  $m = 15$ ,  $r_c/R_\odot = 0.71$ . With the exception of the tesseral Rossby modes mentioned earlier, these modes are the least damped in a wide frequency range as evidenced by their color and symbol size in Fig. 2. In the following we refer to these modes as the *main branch*. Modes on this branch, and with  $r_c/R_\odot = 0.71$ , are marked with black circles. They appear also on Fig. 1 labeled as ‘inertial modes, numerical’. A *secondary* branch, with higher damping and lower frequencies in magnitude can also be identified. It corresponds to the branch with a mode at  $\omega/\Omega_\odot \sim -0.55$  (for  $m = 4$ ,  $r_c/R_\odot = 0.71$ ). Again, as  $m$  increases, their frequency progressively decreases in magnitude until reaching  $\omega/\Omega_\odot \sim -0.35$  at  $m = 15$ . Modes on the main branch have the particular property that their toroidal ( $l = m + 1, m$ ) component near the solar surface is dominant, matching the observed waves, while the modes on the secondary branch have a dominant toroidal ( $l = m + 3, m$ ) component near the surface. In Fig. 3 we present a side-by-side comparison of the spectral amplitudes near the solar surface ( $r = 0.99R_\odot$ ) between two  $m = 8$  modes on the main branch (left panel) and the secondary branch (right panel) for  $r_c/R_\odot = 0.71$ .

Modes in the main branch appear as mainly toroidal from the surface, but they harbor a substantial poloidal component deep in the convective zone. The meridional cross sections in Fig. 4 illustrate this point. Color indicates the dimensionless velocity for each spherical coordinate direction (note that, as a result of an eigenvalue calculation, the overall amplitude of the eigensolution is arbitrary). Modes in the main branch appear to have no radial nodes while the modes in the secondary branch appear to have one radial node. This suggests that the other weaker branches visible in Fig. 2 represent branches with an increasing number of radial nodes.

Lastly, there is a correspondence between the modes in the main branch and a particular class of inertial modes of a full sphere. The inertial modes in a full sphere can be computed analytically (Greenspan 1968; Zhang et al. 2004), and can be specified by three indices ( $\nu, \mu, \kappa$ ), following the notation used by Greenspan (1968). The modes on the main branch reduce to the only retrograde eigenmodes of the full sphere with  $\nu = m + 2$  and  $\kappa = m$  when  $r_c = 0$ . These analytical frequencies are plotted in Fig. 1 as hollow green circles.

#### 4. DISCUSSION

The inclusion of turbulent viscous diffusion in our model give us the ability to discern which eigenmodes are more likely to be excited, although it does not tell us anything about the excitation mechanism itself. As explained earlier, we have tuned the Ekman number  $E$  in order to match the mean damping rate of the  $m = 8, \dots, 14$  eigenmodes in the main branch with one-half of the mean line width of the observed HFR waves. This amounts to an effective viscosity  $\nu_{\text{eff}} \simeq 146 \text{ km}^2/\text{s}$ . There is no direct way of measuring the value of the effective viscosity in the solar interior. As a matter of fact, it may be anisotropic and scale dependent. However, observational and theoretical estimates of the turbulent magnetic diffusivity at the solar surface find values of the order of  $100 \text{ km}^2/\text{s}$  (e.g. Abramenko et al. 2011; Skokić et al. 2019; Baumann et al. 2004). Thus, by assuming that the turbulent magnetic Prandtl number is about unity, our choice is entirely consistent.

For low  $m$  values ( $4 \leq m \leq 8$ ), the modes we find in the main branch are the second least damped after the tesseral Rossby mode family, while at higher  $m$  the main branch becomes the least damped. As shown in Fig. 1, the observed HFR wave frequencies are a fairly close match to the eigenfrequencies of the inertial modes in the main branch, with a small systematic difference. In our model the Sun is rotating uniformly, so it is entirely plausible that a more refined model with differential rotation and/or meridional circulation might explain the frequency difference. The functional dependence of the observed and numerical frequencies with respect to the azimuthal wave number  $m$  is nevertheless nearly identical.

Another important piece of evidence is provided by the spherical harmonic components. The eigenmodes in the main branch are characterized by their dominant ( $l = m + 1, m$ ) spherical harmonic component of radial vorticity near or at the solar surface (see Fig. 3, left panel), precisely like the observed HFR waves. Although the toroidal component is dominant near the surface, the ratio of toroidal to poloidal kinetic energy over the whole convective zone is not far from unity, indicating the presence of substantial flows in the radial direction deep below the surface. The meridional cross sections presented in Fig. 4 provide an illustrative example.

It is tempting to adjust  $r_c$  to match the observed frequencies but it cannot be done consistently for all  $m$  numbers. A glance at Fig. 2 reveals that modes with low  $m$  numbers are much more sensitive to  $r_c$  than modes with higher  $m$ . However, we cannot rule out entirely the possibility that modes with different  $m$  numbers ‘perceive’ a differently sized shell cavity, perhaps related in

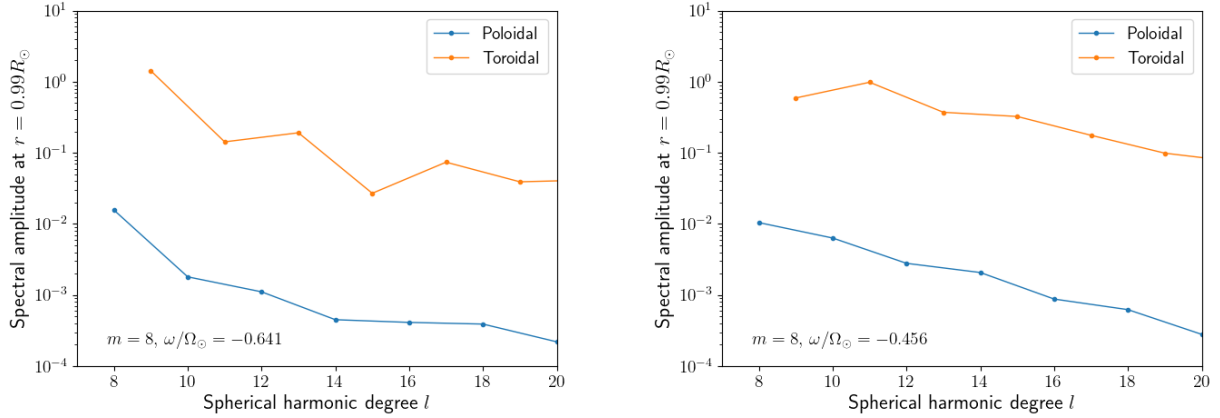


**Figure 3.** Comparison of spherical harmonic amplitudes of the flow velocity at  $r = 0.99R_{\odot}$  between one mode on the main branch ( $\omega/\Omega_{\odot} = -0.641$  on the left), and another mode on the secondary branch ( $\omega/\Omega_{\odot} = -0.456$  on the right). The outer radius of the radiative core is  $r_c = 0.71R_{\odot}$ , the azimuthal wave number is  $m = 8$  and the Ekman number is  $E = 1.06 \times 10^{-4}$ . See middle row, leftmost panel on Fig. 2. Note that the  $(l, m)$  spherical harmonic component of the radial vorticity is proportional to  $l(l+1)T_{lm}(r)/r$ .

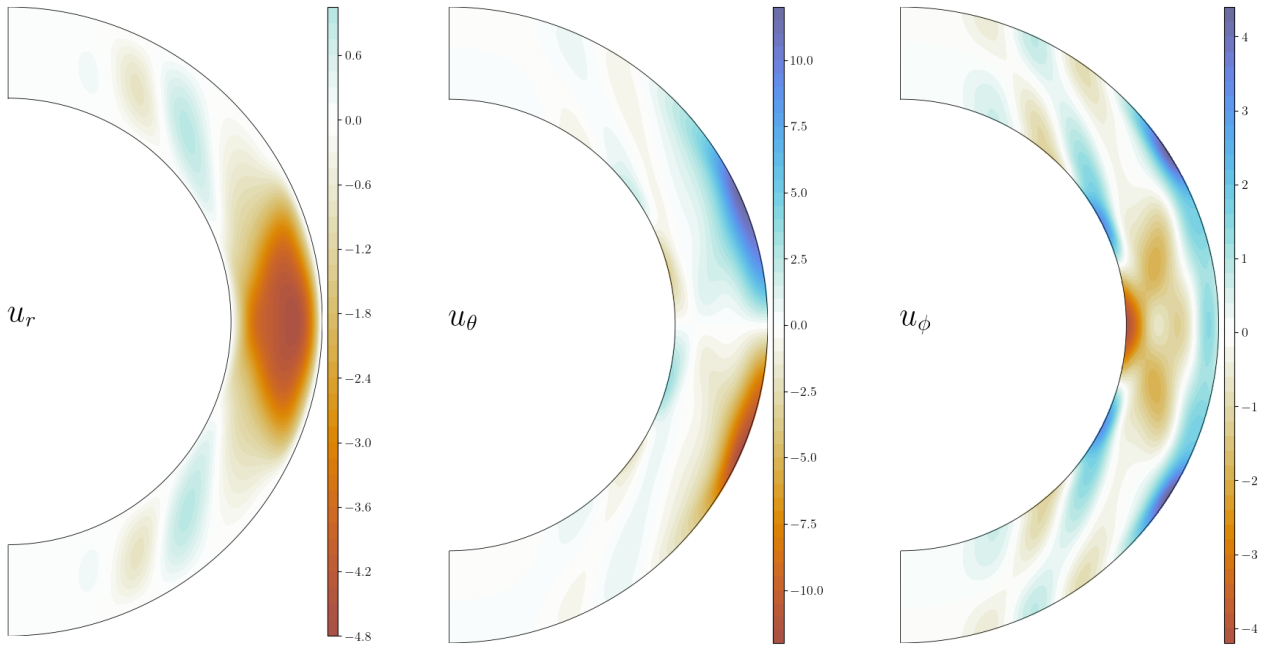


**Figure 4.** Meridional cross sections of the three (dimensionless) velocity components of the  $m = 8$ ,  $\omega/\Omega_{\odot} = -0.641$  eigenmode on the main branch. Ekman number is  $E = 1.06 \times 10^{-4}$  and the outer radius of the radiative core is  $r_c = 0.71R_{\odot}$ . The spherical harmonic spectrum of this mode near the solar surface is shown on the left panel of Fig. 3. Note the absence of radial nodes between the radiative core and the surface.

some way to the meridional circulation pattern in the solar convective zone. Nonetheless, we believe that accounting for the latitudinal differential rotation should be the first refinement to be investigated.

It is interesting to note that the phase speed frequency  $(\omega/2\pi)/m$  of the modes, in the range of 13 to 85 nHz in the retrograde direction, opens the possibility of *co-rotation resonances* of the modes with the background latitudinal differential rotation (Baruteau

& Rieutord 2013; Guenel et al. 2016). In a reference frame co-rotating with the solar equator at a rate of  $\Omega_{\odot}/2\pi = 453.1$  nHz, the latitudinal differential rotation appears as retrograde azimuthal flow with an angular rotation rate decreasing continuously from  $\simeq 120$  nHz near the poles until vanishing at the equator. There is therefore a region in the convective zone in which the Doppler-shifted frequency vanishes for each mode. It is then conceivable that the modes draw their energy from

the differential rotation. That being said, there is presumably some kind of interaction between the large-scale convective flow and the inertial waves with comparable time and length scales. In fact, at  $m > 15$  the waves appear indistinguishable from convection according to Löptien et al. (2018). Thus, an adequate understanding of the interplay among differential rotation, waves, and large scale convection is desirable.

The retrograde ( $l = m + 1, m$ ) tesseral Rossby modes in our model have rather small damping rates, particularly at low  $m$ , which makes them candidates as well to be excited and observed. The power spectra presented by Hanson et al. (2022) (see their Fig. 1) shows indeed some power at low frequencies and low  $m$  numbers in the  $l = m + 1$  channel, which might contain the signature of the tesseral Rossby modes. Although it is not clear if the observed power in that region is not caused by noise or some other artifact. These tesseral Rossby modes have a ratio of toroidal to poloidal kinetic energy much larger than one (a distinguishing feature of *all* Rossby modes), in contrast to the modes in the main branch. They are mostly columnar, with very little amplitude in the equatorial region as Fig. 5 shows. According to our calculations, their spherical harmonic spectra at the surface shows significant contributions from the toroidal  $l = m + 1, m + 3, m + 5$  and higher components which matches, at least qualitatively, the data shown in Fig. S4 of Hanson et al. (2022).

Clearly, the dispersion relation (8) fails to hold for tesseral Rossby modes in a deep spherical shell, although it still holds for *sectoral* Rossby modes, regardless of the shell depth. The latter are purely toroidal (i.e. purely horizontal fluid displacements) and their frequency or damping are essentially unaffected by the shell depth. The tesseral Rossby modes with symmetric vorticity, in addition to the sectoral ones, exhibit similar behaviour as the tesseral Rossby modes with antisymmetric vorticity. As demonstrated by the  $m = 4$  panel in Fig. 2, their frequency is no longer described by the dispersion relation (8) and they become increasingly damped as the shell depth increases. This might explain the apparent lack of symmetric vorticity modes other than sectoral Rossby in the analysis by Löptien et al. (2018).

To conclude this section, we note that the Ekman number has a strong influence on the damping rates while only a weak influence on the eigenfrequencies. But even if the Ekman number is reduced considerably, the tesseral Rossby modes and the modes on the main branch persist as the least damped ones, and the identification of the observed vorticity waves as modes on the main branch remains valid.

## 5. SUMMARY AND CONCLUSION

We presented evidence supporting the identification of the high frequency retrograde (HFR) vorticity waves measured recently by Hanson et al. (2022) as a particular class of inertial modes of a deep spherical shell. Our findings are based on a relatively simple numerical model representing the solar convective zone as a homogeneous, incompressible and viscous fluid in a rotating spherical shell. The eigenmodes of this system correspond to oscillations where the Coriolis force is the restoring force. We recover the Rossby mode frequencies described by the well-known dispersion relation (8) but only for sectoral Rossby modes. We find that Rossby modes other than sectoral are also well described by Eq. (8) but only if the depth of the spherical shell is thin compared to its outer radius. Such a thin fluid layer is hardly justifiable for the solar convection zone. Notably, our model also unveils a branch of lightly damped, retrograde-propagating inertial modes with equatorially antisymmetric vorticity, whose dominant spherical harmonic components  $T_{lm}(r)Y_l^m$  near or at the surface are such that  $l = m + 1$ , and have frequencies fairly close to the wave frequencies observed by Hanson et al. (2022). All of these qualities match observations, leading us to an unequivocal identification of the HFR waves.

The modes we identify with the HFR waves belong to another class of inertial modes, distinct from Rossby modes. Although, as just explained, their dominant component is the toroidal ( $l = m + 1, m$ ) near or at the solar surface, their poloidal kinetic energy is comparable to the toroidal one if we consider the whole convective zone volume.

Our numerical calculations also suggest that the signature of low frequency tesseral Rossby modes with antisymmetric vorticity is present in the observations presented by Hanson et al. (2022). As true Rossby modes, their kinetic energy over the whole convective zone is mostly toroidal, in contrast with the modes in the main branch. Near the solar surface the tesseral Rossby modes have spherical harmonic ( $l, m$ ) components with contributions from  $l = m + 1, m + 3, m + 5$ , and higher orders to a lesser extent, which appears to match the observations as well.

Differential rotation is perhaps the most important feature lacking in our model preventing an optimal match with the observed frequencies. However, it is not essential for the identification of the modes. Our aim here is to provide the initial identification of the modes as a starting step towards more refined models, hoping to spark interest from the community in developing inertial wave models involving differential rotation, magnetic fields, and other effects. Such models, although

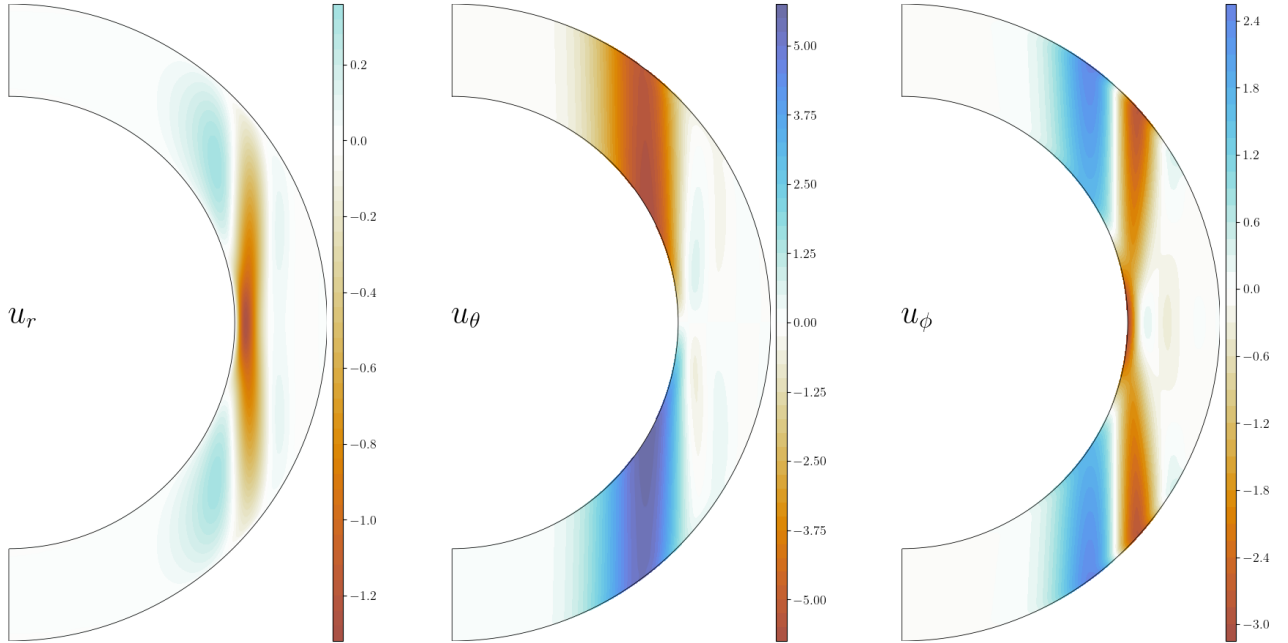


**Figure 5.** Meridional cross section of the  $m = 8$ ,  $\omega/\Omega_{\odot} = -0.118$  mode. This is a *tesseral Rossby* mode. Ekman number is  $E = 1.06 \times 10^{-4}$  and the outer radius of the radiative core is  $r_c = 0.71R_{\odot}$ . See middle row, leftmost panel on Fig. 2.

numerically challenging, are in principle straightforward to develop. More refined inertial wave models are potentially very valuable to understand and characterize turbulent processes in the solar convective zone (Gizon et al. 2021; Bekki et al. 2022), but just as well in the convective zones of other stars where oscillations in the inertial range have been detected (e.g. Ouazzani, R.-M. et al. 2020). Inertial-wave-based helio/asteroseismology has great potential and might give us new insights into the interior dynamics of the Sun and the stars.

- 1 S. Triana. and J. Requier express their warm gratitude to
- 2 V. Dehant and T. Van Hoolst for their encouragement
- 3 and support. They also acknowledge financial support
- 4 from the European Research Council (ERC) under the
- 5 European Union’s Horizon 2020 research and innova-
- 6 tion program (Synergy Grant agreement no. 855677
- 7 GRACEFUL). A. Barik would like to thank Sabine
- 8 Stanley for her encouragement and support.

*Software:* `kore` (Triana et al. 2019; Requier et al. 2019), `SHTns` (Schaeffer 2013), `PETSc/SLEPc` (Balay et al. 2019, 1997; Dalcin et al. 2011; Hernandez et al. 2005; Roman et al. 2021), `MUMPS` (Amestoy et al. 2001, 2006), `Matplotlib` (Hunter 2007).

## APPENDIX

### A. NUMERICAL METHOD

We expand the poloidal  $P_{lm}(r)$  and toroidal  $T_{lm}(r)$  functions occurring in Eq. (4) using a Chebyshev polynomial basis. We write

$$P_{lm}(r) = \sum_{k=0}^N \alpha_{lm}^k t_k(x), \quad T_{lm}(r) = \sum_{k=0}^N \beta_{lm}^k t_k(x), \quad (\text{A1})$$

where  $t_k(x)$  is the Chebyshev polynomial of degree  $k$ ,  $N$  is the radial truncation level, the radial variable is mapped to  $x$  via the affine transformation

$$x = 2 \frac{r - r_c}{R_{\odot} - r_c} - 1, \quad (\text{A2})$$

and  $\alpha_{lm}^k, \beta_{lm}^k$  are the unknown coefficients. We use a fast spectral method devised by [Olver & Townsend \(2013\)](#) that uses Gegenbauer polynomials bases to represent the radial derivatives of  $t_k(x)$ . The resulting matrices representing Eq. (1) are banded and sparse. We end up with a generalized eigenvalue problem of the form

$$\mathbf{A}\mathbf{x} = \lambda\mathbf{B}\mathbf{x}, \quad (\text{A3})$$

where  $\mathbf{A}$  and  $\mathbf{B}$  are sparse matrices,  $\lambda = (\sigma - i\omega)/\Omega_\odot$  is the eigenvalue, and  $\mathbf{x}$  is the eigenvector comprised by the set of coefficients  $\{\alpha_{lm}^k, \beta_{lm}^k\}$ . We use a *shift and invert* strategy to obtain solutions with an eigenvalue close to a given target. The truncation levels used in our calculations are typically  $N = 156$  and  $l_{\max} = 158$  for the radial and angular expansions, respectively.

Our code `kore` is freely available as an open-source project via this link: <https://bitbucket.org/repepo/kore/>.

## REFERENCES

- Abramenko, V. I., Carbone, V., Yurchyshyn, V., et al. 2011, *ApJ*, 743, 133, doi: [10.1088/0004-637X/743/2/133](https://doi.org/10.1088/0004-637X/743/2/133)
- Amestoy, P. R., Duff, I. S., L'Excellent, J.-Y., & Koster, J. 2001, *SIAM Journal on Matrix Analysis and Applications*, 23, 15
- Amestoy, P. R., Guermouche, A., L'Excellent, J.-Y., & Pralet, S. 2006, *Parallel Computing*, 32, 136
- Andersson, N. 1998, *Astrophys. J.*, 502, 708, doi: [10.1086/305919](https://doi.org/10.1086/305919)
- Balay, S., Gropp, W. D., McInnes, L. C., & Smith, B. F. 1997, in *Modern Software Tools in Scientific Computing*, ed. E. Arge, A. M. Bruaset, & H. P. Langtangen (Birkhäuser Press), 163–202
- Balay, S., Abhyankar, S., Adams, M. F., et al. 2019, *PETSc Users Manual*, Tech. Rep. ANL-95/11 - Revision 3.11, Argonne National Laboratory
- Baruteau, C., & Rieutord, M. 2013, *Journal of Fluid Mechanics*, 719, 47
- Baumann, I., Schmitt, D., Schüssler, M., & Solanki, S. K. 2004, *A&A*, 426, 1075, doi: [10.1051/0004-6361:20048024](https://doi.org/10.1051/0004-6361:20048024)
- Bekki, Y., Cameron, R. H., & Gizon, L. 2022, arXiv preprint arXiv:2203.04442
- Dalcin, L. D., Paz, R. R., Kler, P. A., & Cosimo, A. 2011, *Advances in Water Resources*, 34, 1124, doi: <http://dx.doi.org/10.1016/j.advwatres.2011.04.013>
- Gizon, L., Cameron, R. H., Bekki, Y., et al. 2021, *Astronomy & Astrophysics*, 652, L6
- Greenspan, H. 1968, *The Theory of Rotating Fluids*, Cambridge Monographs on Mechanics (Cambridge University Press)
- Guenel, M., Baruteau, C., Mathis, S., & Rieutord, M. 2016, *Astronomy & Astrophysics*, 589, A22
- Hanson, C. S., Hanasoge, S., & Sreenivasan, K. R. 2022, *Nature Astronomy*, doi: [10.1038/s41550-022-01632-z](https://doi.org/10.1038/s41550-022-01632-z)
- Hathaway, D. H., & Upton, L. A. 2021, *ApJ*, 908, 160, doi: [10.3847/1538-4357/abc bfa](https://doi.org/10.3847/1538-4357/abc bfa)
- Hernandez, V., Roman, J. E., & Vidal, V. 2005, *ACM Trans. Math. Software*, 31, 351, doi: <https://doi.org/10.1145/1089014.1089019>
- Hunter, J. D. 2007, *Computing in Science & Engineering*, 9, 90, doi: [10.1109/MCSE.2007.55](https://doi.org/10.1109/MCSE.2007.55)
- Lockitch, K. H., & Friedman, J. L. 1999, *The Astrophysical Journal*, 521, 764
- Löptien, B., Gizon, L., Birch, A. C., et al. 2018, *Nature Astronomy*, 2, 568, doi: [10.1038/s41550-018-0460-x](https://doi.org/10.1038/s41550-018-0460-x)
- Michel, C., & Rivière, G. 2011, *Journal of the Atmospheric Sciences*, 68, 1730
- Olver, S., & Townsend, A. 2013, *SIAM Review*, 55, 462
- Ouazzani, R.-M., Lignières, F., Dupret, M.-A., et al. 2020, *A&A*, 640, A49, doi: [10.1051/0004-6361/201936653](https://doi.org/10.1051/0004-6361/201936653)
- Rekier, J., Trinh, A., Triana, S., & Dehant, V. 2019, *Geophysical Journal International*, 216, 777
- Rieutord, M. 2014, *Fluid dynamics: an introduction* (Springer)
- Roman, J. E., Campos, C., Dalcin, L., Romero, E., & Tomas, A. 2021, *SLEPc Users Manual*, Tech. Rep. DSIC-II/24/02 - Revision 3.16, D. Sistemes Informàtics i Computació, Universitat Politècnica de València
- Schaeffer, N. 2013, *Geochemistry, Geophysics, Geosystems*, 14, 751, doi: [10.1002/ggge.20071](https://doi.org/10.1002/ggge.20071)
- Skokić, I., Brajša, R., Sudar, D., Ruždjak, D., & Saar, S. 2019, *The Astrophysical Journal*, 877, 142
- Triana, S. A., Dumberry, M., Cébron, D., et al. 2021, *Surveys in Geophysics*, 1
- Triana, S. A., Rekier, J., Trinh, A., & Dehant, V. 2019, *Geophysical Journal International*, 218, 1071
- Zhang, K., Liao, X., & Earnshaw, P. 2004, *Journal of Fluid Mechanics*, 504, 1–40, doi: [10.1017/S0022112003007456](https://doi.org/10.1017/S0022112003007456)